Acta Cryst. (1977). A**33**, 126–133

Identification of Enantiomorphously Related Space Groups by Electron Diffraction

BY P. GOODMAN AND T. W. SECOMB

Division of Chemical Physics, CSIRO, PO Box 160, *Clayton, Victoria, Australia* 3168

(*Received* 7 *June* 1976; *accepted* 17 *August* 1976)

A simple procedure is presented for the identification of enantiomorphous space groups by electron diffraction. This is based on the ability to determine the sense of an asymmetry in a projection, which is a property of N-beam dynamic diffraction. The steps in this procedure follow those of the X-ray procedure which depends upon anomalous dispersion instead of dynamic scattering. To illustrate and test the electron-diffraction procedure, a space-group determination was carried out on a sample of dextrorotatory α-quartz: space group $P3_221$ was found, in agreement with the findings of de Vries [*Nature, Lond.* (1958), **181**, 1193].

I. Description of the problem

The problem of distinguishing between enantiomorphous space groups is in principle more difficult than the rest of space-group analysis, and the feasibility of a simple electron-diffraction analysis for this problem was recently raised by Grossbard & Moodie (1974). Although the property of handedness is three-dimensional, in crystallography the problem of identification is soluble in projection and involves a determination of the direction of a structural asymmetry, which in X-ray diffraction is solved with the help of anomalous dispersion (Bijvoet, 1949). Anomalous dispersion introduces the imaginary component (of phenomenological absorption) into the structure factor needed to cause a significant departure from Friedel's law.

In electron diffraction, because of strong N-beam interaction, the non-centrosymmetry in a projection can readily be identified in principle without the action of absorption, which means in practice that it is not necessary in most cases to consider the influence of the absorption, which is always present to some extent. [There are however, some cases, notably $BaTiO_3$ and perhaps other ferroelectrics, where enhancement of asymmetry by absorption is an important factor (Tanaka & Lehmpfuhl, 1972).] This additional power of electron diffraction in relation to the breakdown of Friedel's law means that the point-group symmetry of the two-dimensional pattern is the same as the point-group symmetry of the structure in projection, provided that only zero-layer dynamic interactions are significant. This allows us to identify readily a lack of mirror symmetry in a projection. To go further and identify the direction of the asymmetry generally requires computation using the parameters of the particular structure (Goodman & Lehmpfuhl, 1968). Determination of three-dimensional space groups by electron diffraction without this final identification has recently been described in several publications (Goodman, 1975; Buxton, Eades, Steeds & Rackham, 1975; Tinnappel & Kambe, 1975). The remaining problem of identifying enantiomorphous members of space-group pairs then involves the identification of direction in a non-centrosymmetric planar projection, and depends upon our ability to separate the effects of the planar projection symmetry from the remaining three-dimensional effects. This is readily achieved in practice.

The situation with respect to electron diffraction could be summarized as follows. Firstly, it is true that we *actually* have three-dimensional interaction and that in principle one convergent-beam pattern, if sufficiently accurately analysed, could reveal the handedness of the structure. However, if we take the problem in two stages and analyse on the basis of projection symmetries as suggested above, the analysis is not only very much simpler to follow, but deals in first-order rather than second-order effects. The practical example given in § II serves to show this procedure in operation. Table 1 gives the 11 pairs of three-dimensional enantiomorphous space groups in Schönflies and Hermann–Mauguin symbols. With respect to the experimental task of distinguishing between two enantiomorphous members of a pair, these space groups divide into two classes, based on order of difficulty. The three trigonal space-group pairs, containing threefold screw axes, are simpler to distinguish, requiring one determination of direction in an asymmetric projection (the zone-axis projection) followed by a struc-

Table 1. *Listing of the* 11 *three-dimensional enantiomorphous space-group pairs, with both Schönflies and Hermann–Mauguin symbols*

Class	Schönflies		Hermann–Mauguin	
Trigonal	C_3^2	C_3^3	$P3_1$	$P3_2$
	D_3^3	D_3^5	$P3_112$	$P3_212$
	D_3^4	D_3^6	$P3_121$	$P3_221$
Hexagonal	C_6^2	C_6^3	$P6_1$	$P6_5$
	C_6^4	C_6^5	$P6_2$	$P6_4$
	D_6^2	D_6^3	$P6_122$	$P6_522$
	D_6^4	D_6^5	$P6_222$	$P6_422$
Tetragonal	C_4^2	C_4^4	$P4_1$	$P4_3$
	D_4^3	D_4^7	$P4_122$	$P4_322$
	D_4^4	D_4^8	$P4_12_12$	$P4_32_12$
Cubic	O^6	O^7	$P4_332$	$P4_132$

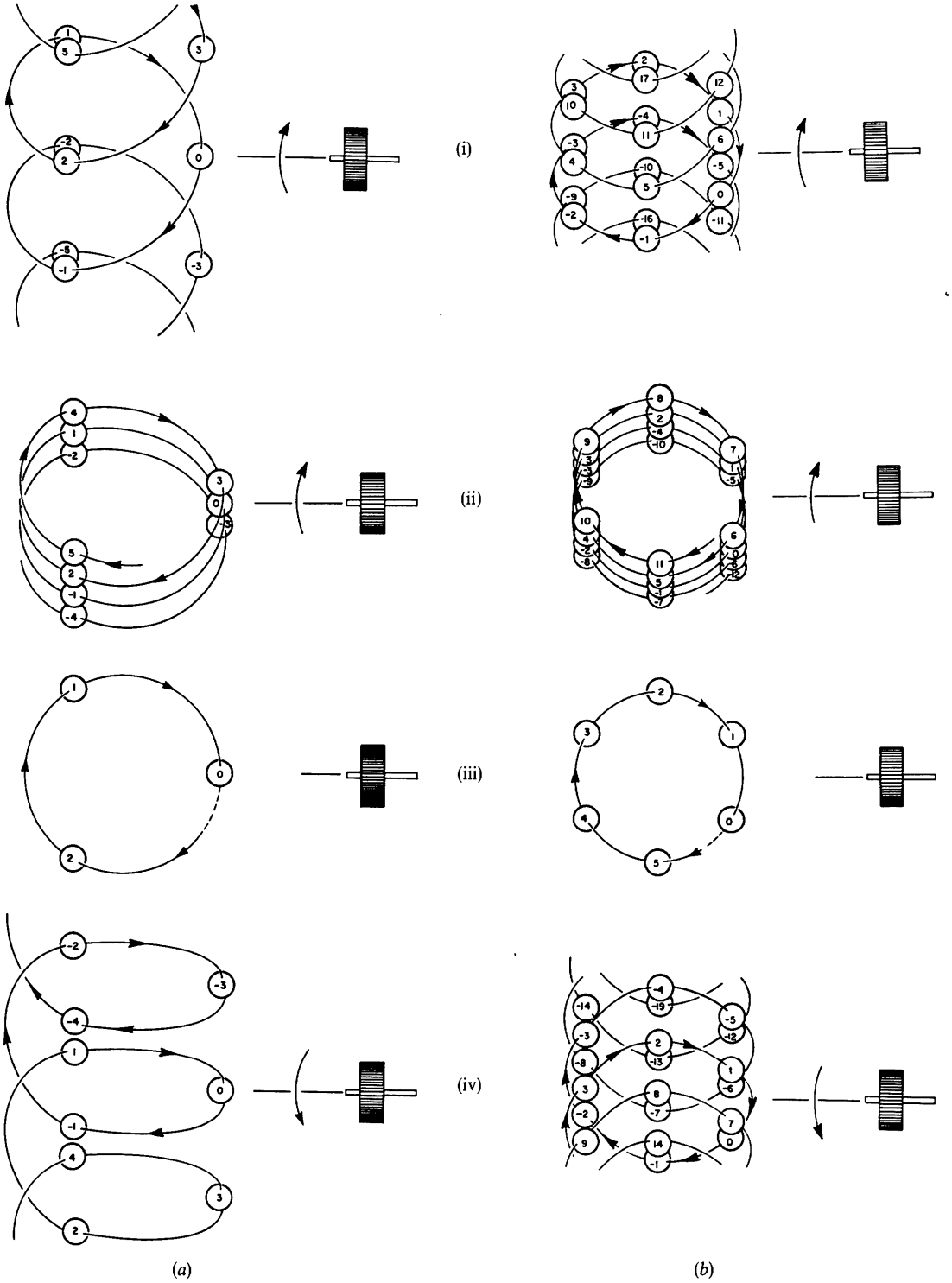

Fig. 1. Projections of (*a*) threefold and (*b*) sixfold helices. The central figures in the two vertical series, numbered (iii), show the axial projection, and the complete series shows the results in projection of rotations from this setting for a helix having a pitch to lateral diameter ratio of 10:8. These rotations are (i) 30° clockwise, (ii) 6° clockwise, (iii) zero, (iv) 30° anticlockwise. The numbers inside the circles show the position of each atom along the helical axis in units of (*a*) 1/3 and (*b*) 1/6 of the pitch.

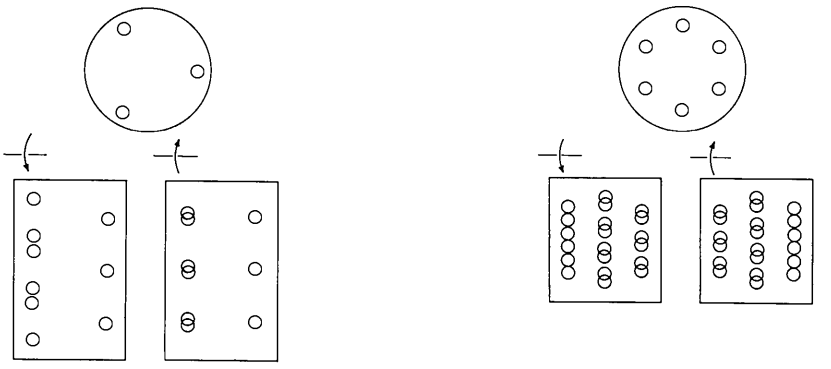

(*c*) (*d*)

Fig. 1 (*cont.*) (*c*) Projection obtained for rotations of $\pm 30°$ for the threefold helix. (*d*) Projection obtained for rotations of $\pm 30°$ for the sixfold helix.

ture-factor determination at another setting. This is to be compared with an identification of direction in two projections which are found by rotation of equal amount and opposite sense from the zone-axis setting required for identification of space groups containing four- and sixfold screw axes. (This identification can be achieved by the determination of direction in one of these non-zone-axis projections.)

This difference in procedure may be understood from projections of models of single helices (Fig. 1). If we take a helical wire and place spheres along it in positions determined by a threefold or a sixfold screw axis we obtain the projections of Fig. 1 (*a*) and (*b*) respectively. The central drawings in the series show the two models with their helical axes vertical; drawings above and below show projections obtained by tilting the models away from this orientation with clockwise and anticlockwise rotations, as indicated. Fig. 1 (*c*) and (*d*) shows results from Fig. 1 (*a*) and (*b*) in simple projection, clearly displaying the different results of equal and opposite rotations in the two cases. In Fig. 1 (*c*) the axial projection for the threefold axis is non-centrosymmetric and has three mirror lines. Provided we can determine the orientation of this projection, *i.e.* discover whether the apex of the triangle is on the left or the right side when one of these mirror lines is set in the horizontal direction of a tilt axis of our goniometer, then the handedness of the model can be determined by standard structure-factor measurement. This is because rotations of opposite senses from the zone axis yield projections which are of different shape and hence have different Fourier *amplitudes*. This is illustrated by the lower projections of Fig. 1(*c*), which are given for the right-handed screw axis. For the left-handed screw axis these projections would be interchanged.

In the case of a sixfold screw illustrated in Fig. 1(*b*) and (*d*) the axial projection is centrosymmetric and is useful in this particular analysis only to show us the position of the six mirror lines. These mirror lines are of two types: three pass through projected 'atoms' while the other three pass between 'atoms'. If we make two equal rotations of opposite senses about a mirror line of the latter type from this setting we now obtain two projections that are mirror images of each other, as shown in Fig. 1(*d*); hence the Fourier components of these projections differ only in *phase*. In crystallographic analysis these two projections must be identified by making use of the breakdown of Friedel's law. The projections obtained in the lower part of Fig. 1(*d*) are obtained for a right-handed screw and would be interchanged for a left-handed screw.

The same considerations apply to a fourfold screw axis as to a sixfold screw axis, since they both give a centrosymmetric axial projection.

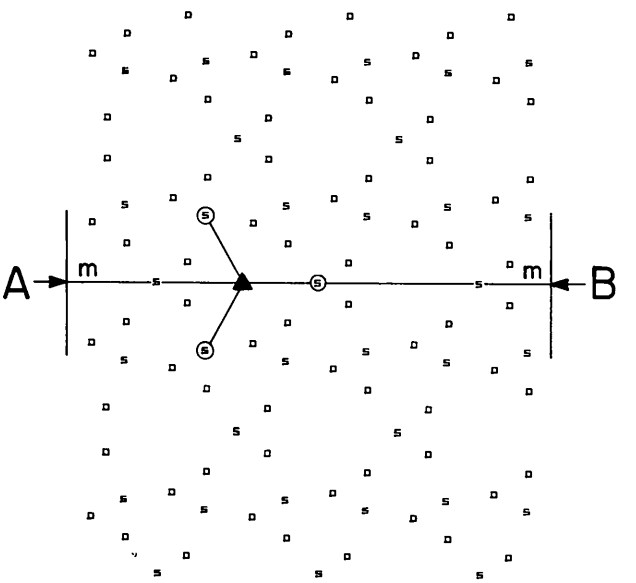

Fig. 2. A representation of the axial projection for α-quartz in which S represents silicon and □ oxygen positions. This diagram has been made without vertical perspective and is valid for both right-handed and left-handed structures. A mirror line of the projection is indicated by the line *m*–*m*. A breakdown in Friedel's law in the diffraction pattern for this zone-axis setting would allow us to distinguish side *A* from side *B* of the crystal.

The complication arising from crystal boundaries which occurs in accurate electron-diffraction analysis can also be understood with optical models by taking a short helix with a partially completed turn. Then the axial projection has only one mirror line (instead of the three, four or six with a completed number of turns). If this mirror line is used for the rotation procedures then the rest of the analysis proceeds as be-

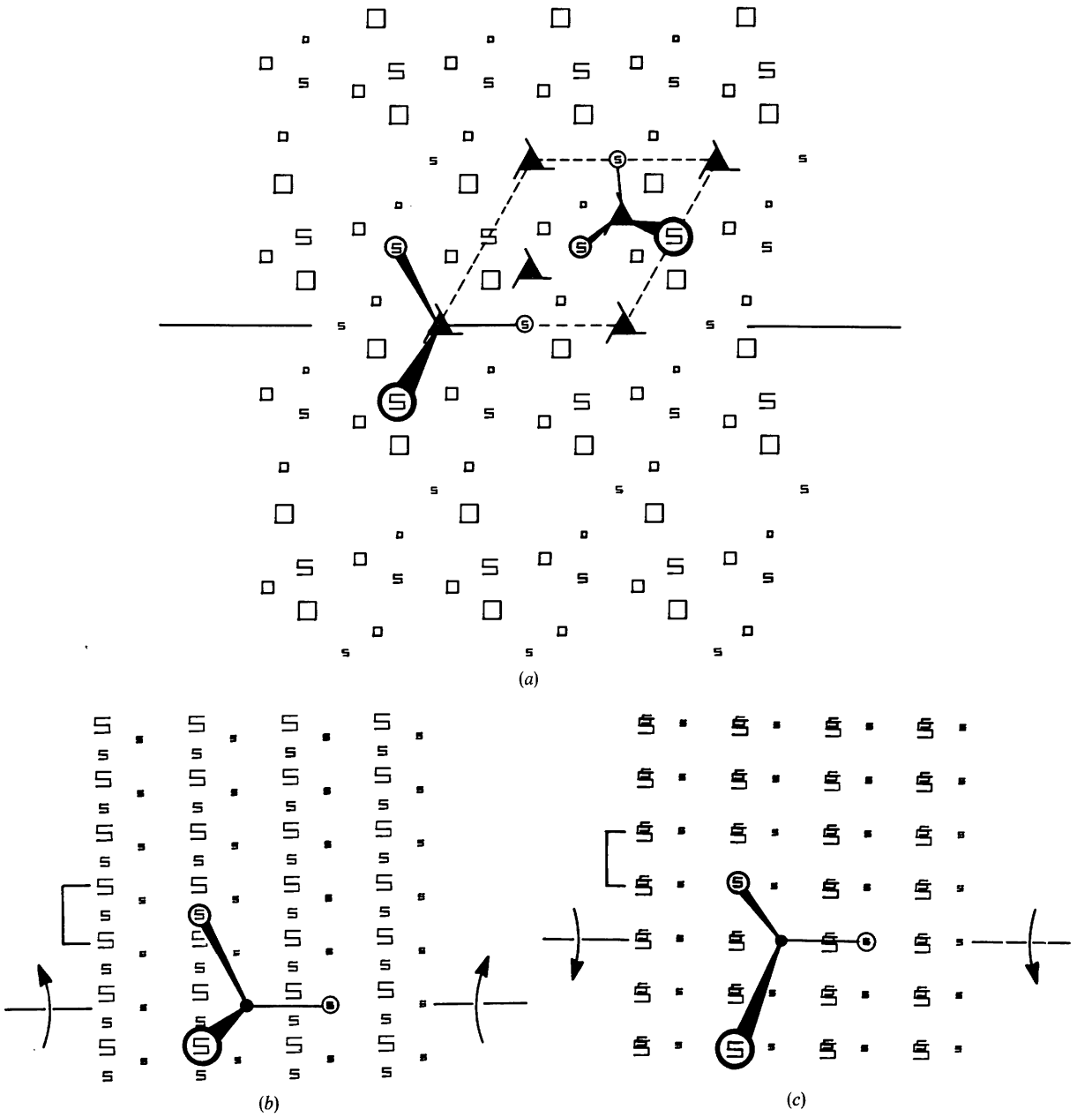

Fig. 3. Perspective computer drawings for α-quartz with the right-handed screw axes of the space group $P3_121$. (*a*) Zone-axis perspective representation showing both Si (S) and O (□) atoms, in which the size of these symbols is made proportional to the *z* coordinate of the atom (height within the unit cell). One unit cell is outlined by a broken line, and the four threefold screw axes within the cell shown. The dispositions of three Si atoms about these axes are shown by perspective drawing in two cases (i) for the wide helix at the origin and (ii) for one of the tight helices within the cell. (*b*) A perspective representation of the structure after a rotation of $+14{\cdot}7°$ from the zone-axis setting and (*c*) A similar representation after a rotation of $-14{\cdot}7°$ from the zone-axis setting (where the signs have the meaning shown in the diagram). To avoid confusion, only Si atoms have been shown in (*b*) and (*c*), since these are sufficient to indicate the result. The rotation axis, indicated by a line either side of the diagrams, has been chosen so as to intersect a screw axis which passes through the unit-cell origin (compare with Fig. 3*a*). The intersection of these two axes is shown as a black dot from which radiate connecting arms to the three related Si atoms (encircled). The perspective representation of this group of atoms unambiguously displays the sense of the $14{\cdot}7°$ rotation; this information is given schematically by arrows at the side of each drawing.

fore. This problem does not arise in our example (§ II), since we are deliberately seeking a method which does *not* depend upon accurate measurement by choosing conditions (including crystal thickness) to obtain a clear intensity asymmetry relatively insensitive to thickness.

The analysis for a single screw axis can be carried over into analysis of space groups containing such screw axes, as illustrated by the following analysis of dextrorotatory α-quartz.

II. Experimental determination of handedness in α-quartz

(*a*) *Identification of projections*

α-Quartz belongs to the pair of enantiomorphous space groups $P3_121$, $P3_221$ (Table 1). The handedness of α-quartz has already been determined by de Vries (1958), who used the anomalous scattering of X-rays, so that our determination might be regarded simply as an illustration of the application of convergent-beam electron diffraction to this problem. Electron diffraction then opens the possibility of future applications to work on microscopic domains beyond the reach of the X-ray method. However, in the course of this investigation there also arose one further problem in addition to those listed in § I. We refer to the double difficulty of following the terminology in the literature and of following the absolute orientation of the crystal during manipulation both on the goniometer and in the associated calculations to avoid making a mistaken identification. The confusion in the literature concerning the nomenclature for α-quartz has been neatly summarized by Lang (1965).

To help in our analysis, we developed an auxiliary computer program for our HP 9830 desk computer which gave a perspective representation of the unit cell (so that the sign of the screw axes could be immediately recognized), and also gave a representation, with unit-cell perspective, of the projection obtained by a specific tilt of the structure about one of the symmetry lines of the [0001] projection. These plotted projections contained information identifying both the sense in which the structure had been rotated from the zone axis and the handedness of the structure, in addition to giving a qualitative picture of the projected potential distribution. This program could either be linked to the structure-factor program, or simply used as in our case to follow the experimental crystal rotations, since the structure-factor values used were sufficiently distinctive to be associated visually with one of the plotted projections. Fig. 2 is a representation of α-quartz without perspective, and is valid for both $P3_121$ and $P3_221$ space groups. The perspective diagrams of Fig. 3 refer to the $P3_121$ space group which contains right-handed screw axes. The single zone-axis projection of Fig. 4 refers to the $P3_221$ space group (with left-handed screw axes).

(*b*) *Procedure*

There are two steps in the experiment. (i) Determination of the absolute orientation of the crystal at the [0001] setting from a convergent-beam zone-axis pattern. This step tells us whether the experimentalist is facing side *A* or side *B* of the projection, as shown in Fig. 2. (ii) Tilt of the crystal about a mirror line of the projection, *i.e.* about a $[11\bar{2}0]$ row, from a [0001] zone axis to suitable settings either side which give distinctive pattern intensities.

These steps may be performed in either order and the combined results will then enable the handedness of the structure to be determined.

(*c*) *Experiment*

(i) A sample of quartz prepared by ion-bombardment thinning was oriented to the [0001] zone-axis setting in a convergent-beam diffraction camera. This setting is obtained when the *c* axis is parallel to the mean incident-beam direction (the direction of the central ray in the incident cone). Convergent-beam patterns then show trigonal symmetry. This trigonality is detectable in the inner reflexions of the zone in two ways. The $11\bar{2}0$ reflexions lying on the mirror lines of the pattern alternate in intensity sequentially around the central, directly transmitted beam, while themselves possessing an internal mirror symmetry. The $10\bar{1}0$ reflexions, which lie between the mirror lines of the pattern possess an internal asymmetry, and this asymmetry alternates in direction around the central

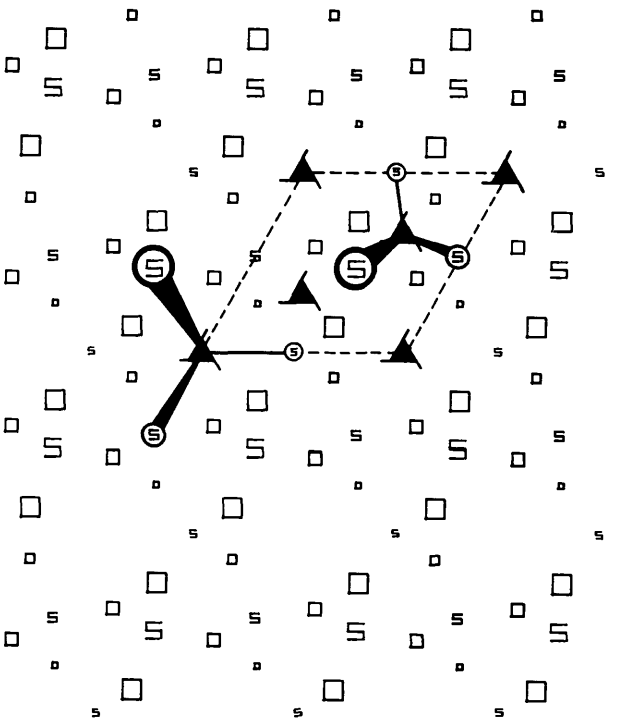

Fig. 4. Perspective representation of the zone-axis projection for the alternative space group $P3_221$ for α-quartz.

beam in a way consistent with a trigonal pattern. Hence, if we wish to measure trigonality (or the degree of departure from hexagonality) from the $11\bar{2}0$ reflexions, we can most conveniently use the central region of the reflexion discs, corresponding to an incident beam parallel to the c axis, whereas measurements of this effect from the $10\bar{1}0$ reflexions must be made from regions near the edges of the reflexion discs, corresponding to a finite inclination of the incident beam to the c axis. Usable crystal thicknesses ranged from about 500 to 5000 Å. Thinner regions showed stronger trigonal symmetry from the $10\bar{1}0$ reflexions and rather weaker $11\bar{2}0$ reflexion intensities, while in thicker regions the trigonality showed up more strongly in the $11\bar{2}0$ reflexions. It was desirable to find a trigonal intensity distribution which had an unambiguous interpretation. Calculations to this end showed that the $10\bar{1}0$ intensity trigonality was most definitive, since the direction of trigonality varied only weakly with thickness. For thicknesses under 1000 Å interpretation of the intensity asymmetry is unambiguous, and in fact this asymmetry shows no substantial reversal for thicknesses up to 2000 Å. This calculated result is shown in Fig. 5. Fig. 6(*a*) shows the pattern obtained from the thinner crystal regions. The arrow on the right-hand side of this figure indicates the direction of view of the operator of the diffraction camera, viewing the pattern from above. The horizontal axis of this picture was chosen as the $[11\bar{2}0]$ axis, about which the crystal was rotated to obtain the results for part (ii) of the investigation. The intensity asymmetry of the pattern together with the results of the calculation shown in Fig. 5 made for points of the pattern identified in the sketch of Fig. 6(*b*), allowed us to identify the absolute orientation. It was thus decided that the left side of the projection of Fig. 2 (labelled *A*) was facing the operator. The fact that the reflexion discs overlap does not invalidate interpretation using Fig. 5, which was calculated for single reflexions. The mirror relation of neighbouring $10\bar{1}0$ discs, plus the addition of *intensities* at points (i) and (ii), simply doubles both intensity values. Fig. 6(*c*) shows the corresponding orientation of those Si sites related by the threefold screw axis at the origin.

(ii) For the final step in the space-group identification we seek pairs of reflexions from the same *hkil* set having structure factors which may be readily distinguished. The $3\bar{3}01$ reflexions provide suitable candidates for this identification since, as pointed out by de Vries (1958), $|V_{3\bar{3}01}| \gg |V_{\bar{3}301}|$ for α-quartz [for the relation between V_{hkil} and F_{hkil} see Dawson, Goodman, Johnson, Lynch & Moodie (1974)]. The direction of the inequality is space-group dependent. In order to determine the direction of this inequality, simple methods of structure-factor measurement can be used since we are no longer, contrary to part (i), concerned with the structural phases α_{hkil}. The α_{hkil} do not enter either the kinematic or the two-beam expressions for diffracted intensity. Consequently, the simple diffraction conditions for which these expressions are approximately applicable, while inadequate for determining structural asymmetry [part (i)], would suffice here.

In classifying reflexions in this section and in Table 2 we use the term 'equivalent reflexions' for reflexions having identical structure-factor *moduli* (as for example $hkil$, $\bar{k}\bar{h}\bar{i}l$, $\bar{h}\bar{k}\,\bar{i}\,\bar{l}$, since $|V_{hkil}| = |V_{\bar{k}\bar{h}\bar{i}l}| = |V_{\bar{h}\bar{k}\bar{i}\bar{l}}|$) and having *hkil* indices belonging to a set of geometrically equivalent reciprocal-lattice points. Such reflexions could also be called 'kinematically equivalent' reflexions. To aid in the interpretation of the next experimental step we list the kinematically equivalent reflexions (Table 2) belonging to the reciprocal lattice rows containing the $3\bar{3}01$ (column 1, Table 2) and $\bar{3}301$ (column 3, Table 2) reflexions, these two named reflexions being non-equivalent and being associated with two distinct projections of the structure.

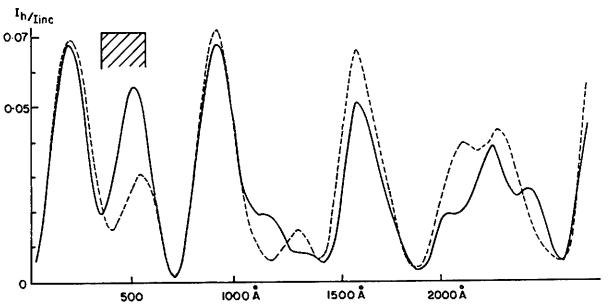

Fig. 5. The result of a 37-beam multislice calculation for the two points (i) and (ii) in Fig. 6(*b*). I_h/I_{inc} (vertical scale) represents the plotted beam intensity I_h for a single $10\bar{1}0$ (full line), and $0\bar{1}10$ (broken line) reflexion, as a fraction of the total incident intensity I_{inc}. The hatched area indicates the only region within the 0–2000 Å range for which the intensity ratio between the beams is greater than 2:1.

Table 2. *The kinematic intensity values,* $|V_{hkil}|^2$, *where the* V_{hkil} *are in volts, shown for three reflexions collinear with the* $3\bar{3}01$*-indexed reflexion in the diffraction pattern for* α*-quartz*

These reflexions are shown encircled in Fig. 7(*a*) and (*b*). Absolute indexing depends on (1) defining the positive direction of the $[11\bar{2}0]$ vector and (2) the space group. If we take the A direction in Fig. 2 as the $[11\bar{2}0]$ direction, then the tabulated values are for the space group $P3_121$. To obtain corresponding values for the space group $P3_221$ columns 2 and 4 must be interchanged.

hkil	$\lvert V_{hkil}\rvert^2$	*hkil*	$\lvert V_{hkil}\rvert^2$
$3\bar{3}01$, $\bar{3}30\bar{1}$	4·24	$\bar{3}301$, $3\bar{3}0\bar{1}$	0·13
$4\bar{2}2\bar{1}$, $\bar{4}22\bar{1}$	0·48	$\bar{4}221$, $4\bar{2}2\bar{1}$	0·48
$2\bar{4}21$, $2\bar{4}2\bar{1}$		$\bar{2}4\bar{2}1$, $2\bar{4}2\bar{1}$	
$5\bar{1}4\bar{1}$, $\bar{5}14\bar{1}$,	0·61	$\bar{5}141$, $5\bar{1}4\bar{1}$,	0·09
$1\bar{5}41$, $\bar{1}54\bar{1}$		$\bar{1}5\bar{4}1$, $1\bar{5}4\bar{1}$	

Under conditions in which N-beam dynamic interactions are important, not only the relative structural phases α_{hkil} but also the scattering geometry is important. Equivalent scattering geometry leads to equiv-

alent accompanying reflexions (called variously 'accidental' or 'weak' reflexions) with equivalent excitation errors in two patterns (*i.e.* 'dynamically equivalent' orientations), but this will lead to exactly the same intensities only if all the structural phases are the same in the two cases. Since the importance of N-beam interactions can to some extent be controlled by choice of crystal orientation, this leads to patterns of varying degrees of complexity, depending upon what is being determined and to what accuracy. Three levels of sophistication which may be employed in practice are illustrated in the following experiment.

If we label the horizontal vector in the diagram of Fig. 6(*a*) as the $[11\bar{2}0]$ axis, then the crystal was rotated about this axis first in an anticlockwise, and then in a clockwise sense, in order to excite firstly the $3\bar{3}0\bar{1}$ reflexion, and then the $3\bar{3}01$ reflexion, corresponding to the two projections shown in Fig. 3. Table 2 lists structure-factor values for these two projections, including values for the $3\bar{3}01$, $4\bar{2}\bar{2}1$ and $5\bar{1}\bar{4}1$-indexed reflexions relevant to the diffraction pictures of Fig. 7(*a*) and (*b*). The tabulated values indicate a ratio for the kinematic intensities of $I_{3\bar{3}01}/I_{3\bar{3}0\bar{1}}$ of 40/1. By relating these tabulated values for an alternatively strong and weak $3\bar{3}01$-indexed reflexion to the projection diagrams of Fig. 3(*b*) and (*c*), which are self-identifying, we can ensure that we have the *hkil* and space-group labelling correct. Fig. 7(*a*) and (*b*) shows the point patterns (obtained with a fine-focus beam having a low angular convergence) obtained from these two settings. It is clear that the encircled reflexions in Fig. 7(*a*) are strong and those in Fig. 7(*b*) are weak. Because of the great difference in the two sets of structure factors and because of the very low values of those of the weak set, the kinematically estimated intensity values are sufficient to identify these patterns in which the excitation errors for the compared reflexions are roughly the same. Combining the identified diffraction diagrams [Fig. 7(*a*) and (*b*)], labelled with the rotation operation employed experimentally, with the distinction between the left and right side of the projection found by part (i) of the experiment shows us that we have the space group $P3_221$, since our actual operations are the opposite of those shown in Fig. 3 for $P3_121$ (and our results opposite to those indicated in Table 2). In other words Fig. 3(*b*) and (*c*) would agree with Fig. 7(*a*) and (*b*) in operation and result if the operator were facing side *B*, and not side *A* as established by Figs. 5 and 6. This result agrees with the established space group for dextrorotatory α-quartz.

Since the excitation-error sets in Fig. 7(*a*) and (*b*) are only approximately equal, a second measurement of a critical reflexion was made as a check. Two higher levels of sophistication in determining these structure factors, made accessible by taking patterns with a wider beam convergence, are illustrated by Figs. 8–10. Firstly, in Fig. 8, we have excited the $\bar{3}301$ reflexion (kinematically equivalent to the $3\bar{3}0\bar{1}$ reflexion: see Table 2) simultaneously with the weak $\bar{2}\bar{2}40$ reflexion, while avoiding excitation of other reflexions of the zone. This pattern contains sufficient information to determine $V_{\bar{3}301}$ to about 10% with the two-beam expression (instead of to within about a factor of two by the kinematic method). Thus the local crystal thickness as determined from the subsidiary maxima spacings within the weakly excited $\bar{1}\bar{1}20$ intensity distribution is 2200 Å. Inspection of the $\bar{3}301$ peak profile shows this value to correspond to approximately $\frac{3}{4}$ of an extinction length (see microdensitometer traces in Fig. 9). These two measurements yield a value for $V_{\bar{3}301}$ of $2{\cdot}0\pm0{\cdot}2$ V. This value is in agreement with the calculated value appropriate to $P3_221$ (see $|V_h|^2$ values in Table 2) and gives further confidence to the space-group identification made above. The $3\bar{3}01$ reflexion was too weak to show effects of extinction in its two-beam profile, but patterns obtained from an orientation near the $[1\bar{1}06]$ zone axis showed stronger dynamic effects. This pattern is shown in Fig. 10. However, interpretation of this type of pattern is unnecessarily complicated for the present problem and was not pursued. Figs. 8–10 simply show the greater effort needed when projections allowing direct identification are not available.

Conclusions

The attempt to distinguish between the space groups $P3_121$ and $P3_221$ for a sample of α-quartz shows that there is indeed a very simple and rapid method for distinguishing between enantiomorphously related

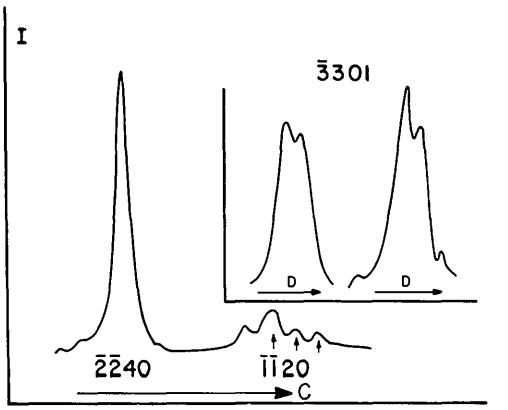

Fig. 9. Relevant microdensitometer scans obtained from Fig. 8. The lower trace, taken in a direction parallel to **C** in Fig. 8, shows the subsidiary maxima from the weakly excited $\bar{1}\bar{1}20$ reflexion. The spacings of these maxima give a crystal thickness $H=2200$ Å, using the kinematic expression. The directly excited $\bar{2}\bar{2}40$ peak occurs on the same trace. The upper traces, shown as an inset, give scans from the $\bar{3}301$ reflexion. These were taken either side of the central third-beam intersection (see Fig. 8) and in a direction parallel to the direction **D** in Fig. 8. If the asymmetry of this peak, arising from N-beam interactions, is ignored an approximate value for $|V_{\bar{3}301}|$ of $2{\cdot}0\pm0{\cdot}2$ V is obtained by means of the two-beam formula.

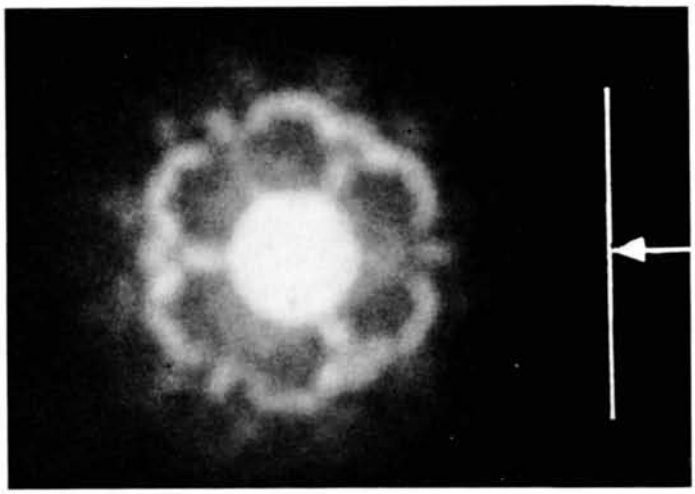

(*a*)

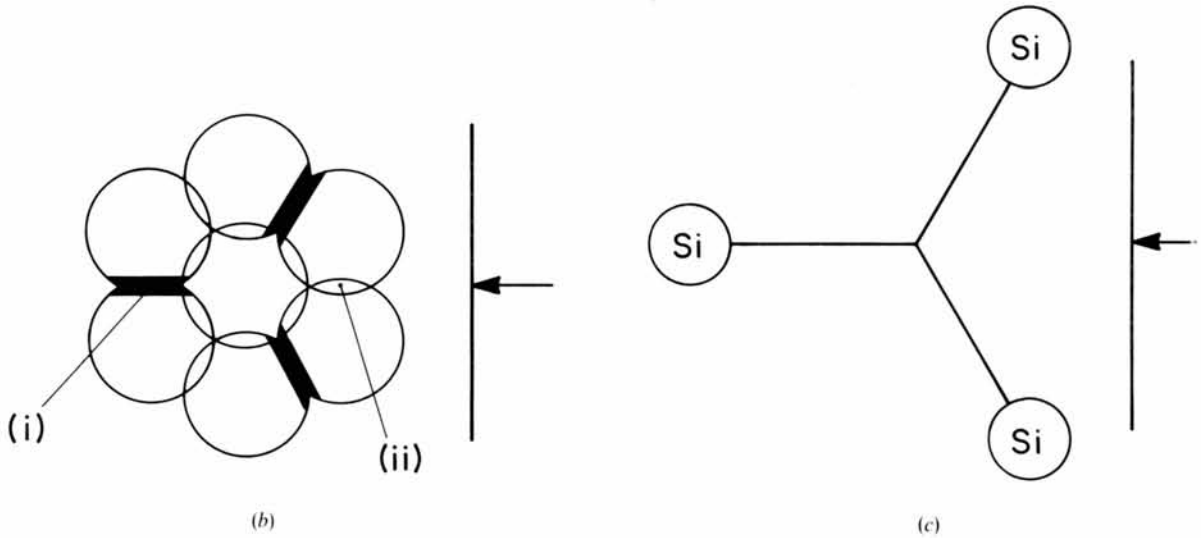

(*b*) (*c*)

Fig. 6. (*a*) Zone-axis convergent-beam diffraction pattern from a thin region of the specimen, showing strong trigonal symmetry in the overlapping first-order reflexions (taken with 80 kV electrons; recorded with Polaroid-Land 3000 ASA film from a transmitting fluorescent screen). (*b*) Graphic representation of the seven main discs in the pattern of Fig. 6 (*a*) shows points (i) and (ii), for which the calculations in Fig. 5 were made. In both (*a*) and (*b*), the arrows indicate the direction of view of the operator of the diffraction camera. (*c*) Representation, in projection, of the three Si atoms that are related by the three-fold axis through the origin of the cell, showing their deduced orientation relative to (*a*) and (*b*).

[*To face p.* 132

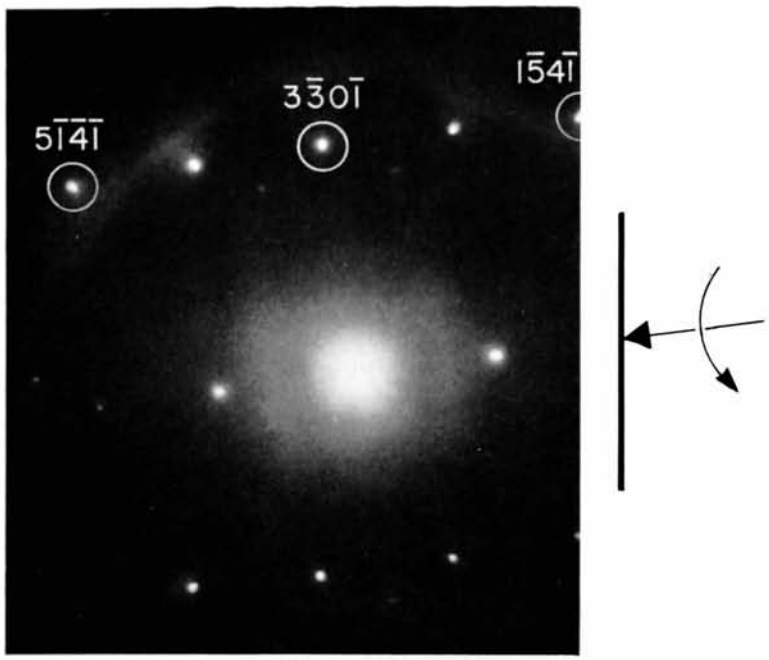

(*a*)

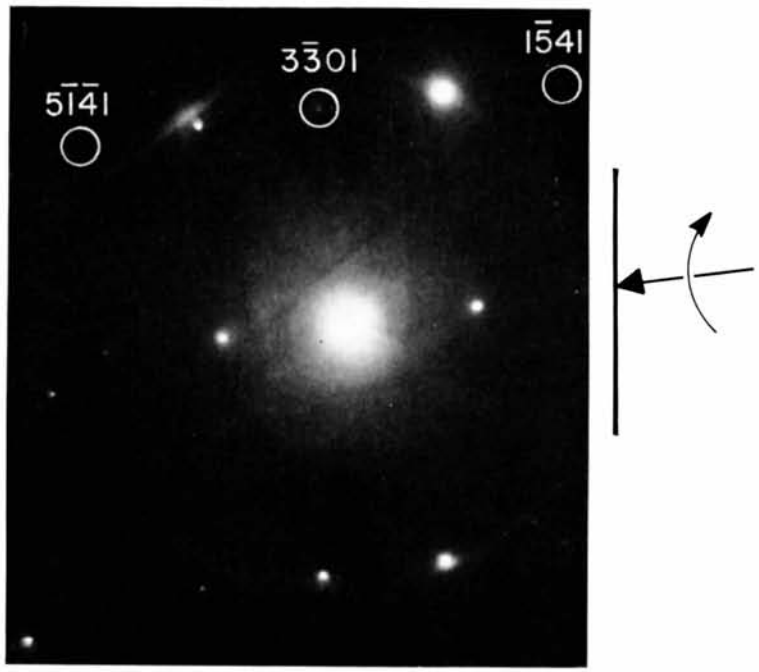

(*b*)

Fig. 7. Point patterns, obtained by a fine-focus beam with a small angular convergence, from orientations of approximately (*a*) $+14{\cdot}7^\circ$ and (*b*) $-14{\cdot}7^\circ$ from the zone-axis setting. These rotations are indicated on the side of the pattern (labelled by a thick line and an arrow) which faced the operator of the diffraction camera. If we take the $[11\bar{2}0]$ vector as being directed away from the operator, the central encircled reflexions are in (*a*) $3\bar{3}0\bar{1}$ and in (*b*) $3\bar{3}01$. The reflexions on either side of $5\bar{1}4\bar{1}$ type index have also been encircled. According to Table 2 these three encircled reflexions are especially sensitive to space group. They are strong in (*a*) and weak in (*b*). Excitation errors are roughly equal in the two photographs as indicated by the positions of the Laue circles. (A different set of accompanying reflexions appears in these two diagrams because the diffraction geometries for exciting the $3\bar{3}0\bar{1}$ and $3\bar{3}01$ reflexions are not equivalent. The same accompanying reflexions *would* occur when exciting, say, the $3\bar{3}0\bar{1}$ and $\bar{3}30\bar{1}$, or $3\bar{3}01$ and $\bar{3}301$ reflexions. This can be seen from the appropriate Ewald diagrams.)

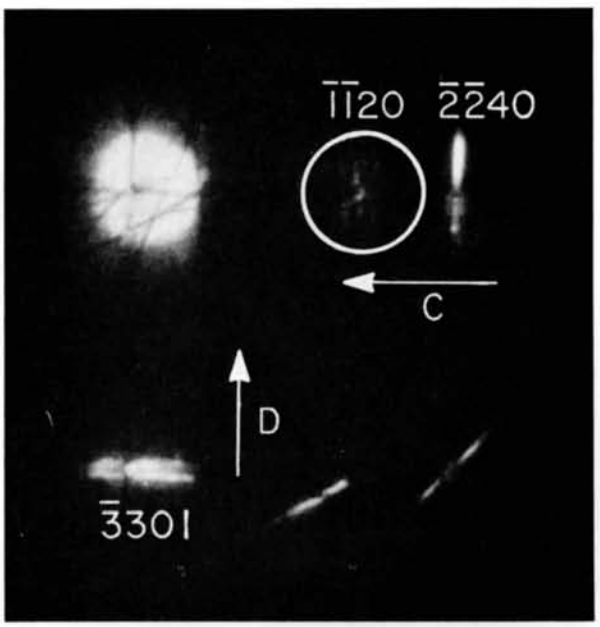

Fig. 8. Convergent-beam diffraction pattern taken so as to excite only the $\bar{3}301$ [equivalent to the strong reflexion of Fig. 7 (*a*)] and $\bar{2}\bar{2}40$ reflexions simultaneously. In this case microphotometer curves from the weakly excited $\bar{1}\bar{1}20$ reflexion (encircled) can be used to determine crystal thickness by scanning in a direction parallel to **C** in this figure, while a profile of the $\bar{3}301$ reflexion, obtained by scanning in a direction parallel to **D**, can be used to determine $|V_{\bar{3}00\bar{1}}|$.

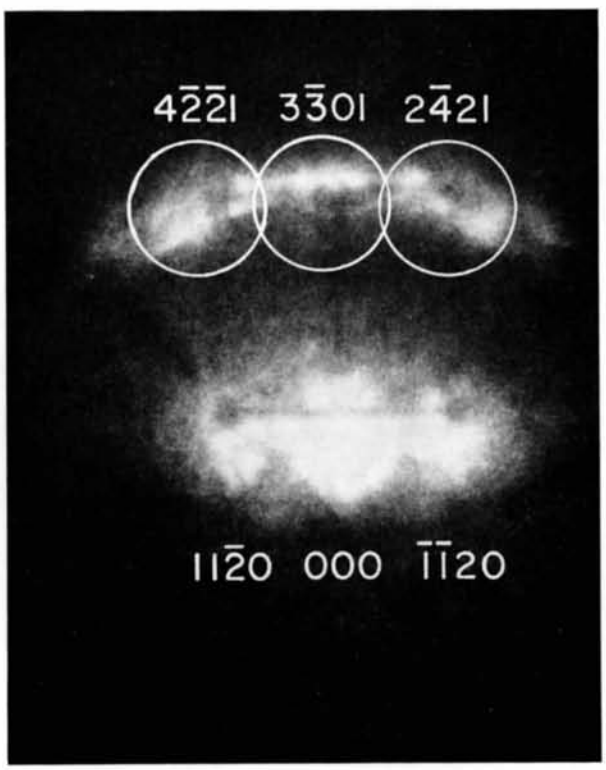

Fig. 10. Convergent-beam pattern showing the $3\bar{3}01$ reflexion [the weak reflexion in Fig. 7(*b*)] excited simultaneously with other reflexions of the local zone.

space groups using convergent-beam electron diffraction, and that this method could be applied to any enantiomorphous space-group problem for substances stable in the electron beam. The relative lack of sophistication needed is emphasized in this particular determination, since all the diffraction pictures which gave the necessary evidence were taken by indirect photography (*i.e.* from outside the vacuum) of a fluorescent screen within an ion-pumped diffraction camera, and are of poorer than conventional quality and resolution.

The authors are indebted to Mr A. F. Moodie for drawing their attention to this problem. In addition, they wish to thank Mr M. Grossbard for obtaining and etching the sample, and Drs A. C. Hurley and A. W. S. Johnson for valuable discussions and for checking the manuscript.

References

BIJVOET, J. M. (1949). *Proc. Roy. Soc., Amsterdam*, **52**, 313.
BUXTON, B. F., EADES, J. A., STEEDS, J. W. & RACKHAM, G. M. (1975). In the press.
DAWSON, B., GOODMAN, P., JOHNSON, A. W. S., LYNCH, D. & MOODIE, A. F. (1974). *Acta Cryst.* A**30**, 297–298.
GOODMAN, P. (1975). *Acta Cryst.* A**31**, 804–810.
GOODMAN, P. & LEHMPFUHL, G. (1968). *Acta Cryst.* A**24**, 339–347.
GROSSBARD, M. & MOODIE, A. F. (1974). International Crystallography Conference, Melbourne. Unpublished.
International Tables for X-ray Crystallography (1965). Vol. 1. Birmingham: Kynoch Press.
LANG, A. R. (1965). *Acta Cryst.* **19**, 290–291.
TANAKA, M. & LEHMPFUHL, G. (1972). *Acta Cryst.* A**28**, S202.
TINNAPPEL, A. & KAMBE, K. (1975). *Acta Cryst.* A**31**, S6.
VRIES, A. DE (1958). *Nature, Lond.* **181**, 1193.

Acta Cryst. (1977). A**33**, 133–136

Extinction-Free Measurements with Plane-Polarized X-rays

BY A. MCL. MATHIESON

Division of Chemical Physics, CSIRO, P.O. Box 160, *Clayton, Victoria, Australia* 3168

(*Received* 29 *June* 1976; *accepted* 11 *July* 1976)

A means of obtaining single-crystal data from which the effects of extinction have been eliminated is described. The method involves the use of plane-polarized X-rays diffracting in the π mode from a crystal plane. Measurements of integrated intensity are made over a range of 2θ on either side of $2\theta = 90°$. A suitably chosen function of the intensities is plotted against a function of 2θ and extrapolated to the limit, $2\theta = 90°$. The prerequisite for this procedure is a source of plane-polarized X-rays of wavelength selectable over a range such as 5 to 0·5 Å, a facility previously difficult to establish but now feasible with synchrotron radiation. The method is discussed in relation to symmetrical Bragg reflexion from an extended-face crystal but is relevant to other cases such as the transmission (Laue) technique or a small crystal bathed in the X-ray beam.

Introduction

In a recent paper, I discussed one experimental procedure (method I) for obtaining single-crystal diffraction data free from extinction, using asymmetric reflexion from extended-face crystals (Mathieson, 1976). While that procedure requires a relatively large crystal specimen and may involve its being shaped and polished, nevertheless the requirements in respect of diffraction equipment are simple.

Further consideration of the basic physical principles underlying the occurrence of extinction has led to the recognition of a second practicable experimental procedure (method II) which is capable of controlled variation so that, in the limit, it yields extinction-free data. Method II involves the use of plane-polarized X-rays diffracting in the π mode (Compton & Allison, 1935) and extrapolation of an appropriate function of the measured intensities to $2\theta = 90°$.

In contrast to method I, method II requires somewhat specialized conditions which, in the past, would have been rather difficult to set up. Now, however, a synchrotron source can provide the necessary prerequisite, namely plane-polarized X-rays of wavelength selectable over a wide range (see, for example, Codling, 1973).

From the discussion which follows, it will be evident that this second method is not as restrictive as the first in terms of size, and especially shape, of the crystal specimen. Hence method II may prove useful in circumstances where method I is not applicable.

Comment on the kinematical theory and extinction

Before dealing with the method, it may be as well to clarify the approach to the question of extinction.

In the literature, one finds that the discussion of kinematical theory varies sufficiently from author to author, depending upon the specific aspect which he wishes to treat, that it would appear advisable to present an explicit statement as to the viewpoint adopted here, namely that the formulae associated with the